LAWRENCE
LIVERMORE
NATIONAL
LABORATORY

LLNL-JRNL-421509

Non-LTE and gradient effects in K-shell oxygen emission laser-produced plasma

J. Colgan, J. Abdallah, C. J. Fontes, D. P. Kilcrease, J. Dunn, M. Purvis, R. W. Lee

December 16, 2009

High Energy Density Physics

Disclaimer

Non-LTE and gradient effects in K-shell oxygen emission laser-produced plasma

J. Colgan[1], J. Abdallah, Jr.[1], C. J. Fontes[2],

D. P. Kilcrease[1], J. Dunn[3], M. Purvis[4], and R. W. Lee[3]

[1] *Theoretical Division, Los Alamos National Laboratory, Los Alamos, NM 87545*

[2] *Applied Physics Division, Los Alamos National Laboratory, Los Alamos, NM 87545*

[3] *Lawrence Livermore National Laboratory, Livermore, CA 94551*

[4] *Department of Electrical and Computer Engineering, Colorado State University, CO 80523*

Abstract

A recent effort [1] to develop a high-resolution spectroscopy capability for He-like and H-like ions to study far wing shapes from a laser-produced plasma experiment at the Lawrence Livermore National Laboratory found unexpected structure in the observed emission from a Mylar target. In this paper we propose that the observed features are due to exotic inner-shell transitions in mid-ionized oxygen, suggesting that the observed emission arises from two plasma regions: a hotter, less dense outer region gives rise to the observed He-like and H-like resonance lines, while a cooler, more dense plasma region closer to the target surface and in a region surrounding the laser spot generates the dielectronic satellites and the exotic inner-shell lines. Calculations using the Los Alamos suite of atomic physics codes and the plasma kinetics code ATOMIC are used to support this assertion.

Preprint submitted to Elsevier Science *7 December 2009*

1 Introduction

Experimental investigations of emissivities and opacities from hot, dense plasma are a vital step in furthering our understanding of the properties of such highly ionized plasmas. Although many theoretical efforts worldwide now exist to model the plasma parameters of such plasmas (for example, the recent NLTE workshop summaries [2–4]), comparison with experiment is crucial in determining how well the physics of the system is described by theory. Unfortunately, such experimental investigations are generally difficult and costly to construct, and the interpretation and diagnosis of the measured quantities is also formidable. However, experiments involving laser-produced plasmas (especially as ever more powerful lasers are utilized), magnetically confined plasmas, and pinches have all contributed important steps towards our understanding of the plasma physics. For example, experimental spectra of Fe obtained from the Z-pinch facility at Sandia National Laboratory were successfully compared to several leading theoretical models [5]. Efforts are also underway at Lawrence Livermore National Laboratory (LLNL) to use the Jupiter Laser Facility to conduct laser-produced plasma experiments with high resolution on low-Z targets [1]. The main thrust of the experimental work is to measure the line shape of the K-shell resonance lines in the wing far from the line center and in a low opacity part of the spectrum. The goal is to determine the intrinsic line shape at different plasma conditions free from other lines to compare with opacity codes and assess the effect on the Rosseland mean opacity [6]. The strong $n = 2$ K-shell lines in low-Z ions are good candidates for study here due to the substantial theoretical and experimental effort that has been performed and the low emission strength of the dielectronic satellites

[7,8].

In this paper, we explore some of the recent results from this effort for oxygen spectra obtained in the 15.0–23.0 Å wavelength range. A short laser pulse of 150 ps (full width at half maximum) using the Compact Multipulse Terawatt (COMET) laser [9] was focused at high irradiance on Mylar ($C_{10}H_8O_4$) and aerogel (SiO_2) targets. Emission lines were spectrally resolved from K-shell oxygen with high spectral resolution and high dynamic range. Emission lines from C and H are not expected to occur in this wavelength range. The high spectral resolution in the experiment made possible the observation of satellite lines up to $n = 7$ or 8 from both targets, and the usual He-like lines (including the intercombination line) were also well resolved. However, additional lines were observed in the spectra from the Mylar target that were not seen in the spectra from the aerogel target. In this paper, we attempt to explain these extra features and postulate that they arise from a portion of the plasma that is colder and denser than the bulk plasma. We use the Los Alamos suite of atomic physics codes and the plasma kinetics code ATOMIC [10] to perform studies of the emissivity from an O plasma for various temperature and density ranges.

2 Experiment

The measurements of the K-shell oxygen spectra were recorded from a laser-heated target on the LLNL COMET facility [1]. This chirped pulse amplification laser can generate several beams simultaneously with pulse durations from 500 fs to 600 ps with a choice of 1ω or frequency-doubled 2ω corresponding to wavelengths of 1054 nm and 527 nm, respectively [9]. A single laser

pulse of duration 250 ps (FWHM), 527 nm wavelength with up to 5 J energy on target was focused with an $f/4.8$ off-axis parabola of focal length 30 cm. The maximum laser irradiance of 5×10^{15} W cm^{-2} was achieved with a laser focus smaller than 20 μm (FWHM) diameter. The vertically polarized laser beam was incident on target at 21.8° from normal. The laser was fired at a repetition rate of 1 shot/4 minutes. The targets under study included 1.5 μm and 3 μm thick Mylar ($C_{10}H_8O_4$) foils and 50 mg cm^{-3} density aerogel (SiO_2) disks 1.4 mm diameter by 300 μm thick.

The spectrometer consisted of a variable-spaced grating of average ruling 2400 line/mm with radius of curvature $R = 44.3$ m [1]. The spectrometer was run with a 10 or 25 μm wide slit placed at a distance of 150 cm from the grating and 56 cm from the plasma. A light-tight 200 nm Al filter was placed behind the slit to prevent scattered light from reaching the detector placed 150 cm from the grating. The grating was inclined at a grazing angle of incidence of approximately 2° vertical to the source. A Princeton Instruments PI-SX camera, liquid-nitrogen cooled, back-thinned CCD with 1340 × 1300 pixels (pixel size 20 × 20 μm^2), and operated at -110 °C, was used with a low noise analog-to-digital-converter to record the spectra. Single-shot spectra with signal-to-noise ratios of 5000 were recorded. The spectrometer viewed the target surface at a grazing angle of 5° in order to minimize Doppler shift expected to be less than 2 mÅ due to plasma expansion normal to the laser target.

Fig. 1 shows the oxygen spectrum with the main K-shell transitions in the 15–23 Å waveband from a laser heated 3μm thick Mylar foil. Three separate spectra were taken under similar conditions and added to further improve the signal-to-noise and statistics of the low intensity dielectronic satellite features

to the long wavelength side of the H-like n = 2–1 line. The strongest lines are labeled as the He-like and H-like oxygen resonance lines and were used to calibrate the dispersion on the instrument using reference wavelengths [11]. A second-order polynomial fit was applied to the spectrum and the overall accuracy of the resonance line positions was determined to be within ± 2–3 mÅ. The strongest He-like dielectronic lines in the 19–19.6 Å band were found to be a little different in wavelength when compared to theoretical calculations [8] and will be reported at a later date. Hydrodynamic simulations for these laser plasma conditions indicated that the plasma electron temperature increases to over 1 keV during the peak of the laser pulse [1,12]. The resonance line spectra are emitted strongly in the recombination phase in the corona at 3–6 $\times$ 10^{20} cm^{-3} electron density as supported by observed cutoff of the high n transitions. However, the dielectronic satellite lines to the long wavelength side of the 18.97 Å O Ly-α resonance line are emitted close to the target surface when viewed with spatially-resolved spectroscopic imaging.

3 Atomic Model

The atomic data used to model the experiment were generated from the Los Alamos suite of computer codes, which have been developed over many years to calculate atomic structure and atomic scattering quantities. The CATS code [13], which is an adaptation of Cowan's atomic structure codes [14], was used to calculate wavefunctions, energy levels, oscillator strengths, and plane-wave Born (PWB) collision strengths for the B-like through the bare ionization stages of O, including the PWB correction at threshold [14]. CATS was used to generate data in the fine-structure approximation and

configuration-interaction was included in the structure calculations for each ion stage. Electron-impact ionization, photoionization, and autoionization cross sections were calculated using the multi-purpose ionization GIPPER code [15]. The latter two processes were calculated explicitly with distorted-wave continuum functions while the electron-impact ionization calculations used scaled hydrogenic cross sections that were designed to accurately reproduce distorted-wave calculations for highly charged ions. More accurate collisional excitation cross sections were also generated via the ACE code [16], using first-order many-body perturbation theory [17,18] for a set of selected levels. Collisional de-excitation, three-body, radiative, and dielectronic recombination rates were obtained from detailed balance.

The atomic model used for this study included almost 10,000 levels, with a significant portion of the levels used to describe the more neutral ion stages. Since it was suspected that the unusual spectral features observed in the experimental spectra could have arisen from exotic transitions, special care was taken to include levels arising from 'hollow-atom' and other multi-excited configurations [19–21]. For the H-like stage, all levels were included up to $n = 7$. For the He-like ion stage, all levels were included arising from configurations of the form $1s^2$, $1s2l$, $1snl$, $2snl$, $2pnl$, with $3 \leq n \leq 7$, as well as levels arising from $(2l)^2$ and $(3l)^2$ configurations (where here and in the following description $(2l)^2$ should be taken to mean all possible two-electron permutations of configurations in the $n = 2$ shell). For the Li-like ion stage, levels were included arising from the configurations $1s^22l$, $1s^2nl$, $1s(2l)^2$, $1s2lnl'$, $1s(3l)^2$, $(2l)^3$, $(2l)^2nl'$, with $3 \leq n \leq 5$. For the Be-like ion stage, levels were included arising from configurations of the type $1s^2(2l)^2$, $1s^22lnl'$, $1s^2(3l)^2$, $1s(2l)^3$, $1s(2l^2)nl'$, $1s(3l^3)$, $(2l)^4$, and $(2l)^3nl'$, with $3 \leq n \leq 5$. Finally, for the

B-like ion stage, levels were included arising from configurations of the type $1s^2(2l)^3$, $1s^2(2l)^2nl'$, $1s^22l(3l')^2$, $1s(2l)^3nl'$, $1s(2l)^4$, $1s2l(3l')^3$, $(2l)^5$, $(2l)^4nl'$, with $3 \leq n \leq 5$. The solution of the rate equations for the O plasma was carried out using the Los Alamos code ATOMIC, which has been described previously [10]. ATOMIC is a multi-purpose plasma kinetics code which can be run in LTE or non-LTE (NLTE) mode to produce a wide range of quantities of interest, such as ion fractions, radiative power losses, opacities, and emissivities. The rate equations may be solved for time-dependent or steady-state conditions. In the present case, the steady-state NLTE rate equations were solved for various electron temperatures and densities as described in the following section. Gaussian line shapes were used for all the calculations described in the following section, unless otherwise noted.

4 Results and Discussion

In the experimental campaign, set up to study low-Z K-shell lines, comparisons were made of spectra obtained from a Mylar target and an aerogel target. The Mylar target starts from a solid density as high as $n_e \sim 4 \times 10^{23}$ cm^{-3}, while the aerogel target starts from a somewhat lower density $n_e \sim 1.5 \times 10^{22}$ cm^{-3} for a fully ionized target. Plasma hydrodynamic motion quickly lowers the density, and in [1] an upper limit of 6×10^{20} cm^{-3} was estimated for the plasma electron density for both targets. One of the more interesting features of this experimental analysis was the appearance of additional lines in Fig. 1 (shown in the blown-up portion in Fig. 1b) in the Mylar spectra, which did not appear in the aerogel spectra. The lines in the 19.1–19.6 Å range are dielectronic satellite lines to the O Lyman-α, but the lines in the 20.0–21.0 Å

were unidentified, with initial conjectures made in [1] that they were possibly due to the presence of a high-Z contaminant. The high-Z contaminant was discounted when the bulk material analysis of the material indicated the highest level impurity was at the 50 ppm level by weight and so would be undetected.

The plasma kinetics code ATOMIC was used to compute the emissivity from O for a range of temperatures and densities, using the model described in the previous section. It was found that NLTE calculations (i.e. with T_r=0) at similar densities to that estimated in [1] and at electron temperatures between 100–150 eV produced spectra that were in reasonable agreement with the broad features of the experimental spectrum. For example, in Fig. 2a, we present a spectrum computed for $T_e = 150$ eV and $N_e = 3.6 \times 10^{20}$ cm^{-3} (solid line). By comparing to Fig. 1, it is seen that the ATOMIC calculation for these conditions produces positions and intensities of the Lyman-α and Lyman-β lines, as well as the He-α line and subsequent members of this series, that are in good agreement with the experimental spectrum. The ATOMIC calculation for these conditions also produces some dielectronic satellite lines in the 19.1–19.6 Å range, but no lines are obtained between 20.0 and 21.0 Å.

For further comparison we also present in Fig. 2a an LTE ($T_r = T_e$) calculation made for the same conditions. The LTE calculation predicts a higher average ionization (of 7.96) than the NLTE calculation (average ionization of 7.11), resulting in much weaker dielectronic satellite lines in the LTE calculation as well as lower intensity He-like lines. The NLTE calculation appears to more closely describe the experimental features. However, it is possible that LTE calculations at lower temperatures may be in better agreement with experiment than the LTE calculation at 150 eV.

Since the calculations for these relatively hot and moderately dense plasma conditions produced no lines between 20 and 21 Å, consideration was given to what transitions could produce lines in this region. It was realized that excited-excited inner-shell transitions in less-ionized O could produce lines in this wavelength range. After some exploration of the spectral lines produced at higher densities and various temperatures, it was found that intense spectral lines are found in the 20.0 to 21.5 Å range for colder and more dense plasma conditions. In Fig. 2b we show a typical spectrum produced from a NLTE calculation using an electron temperature of 60 eV and an electron density of 5×10^{22} cm^{-3}. The lines between 20.0 and 20.5 Å are from excited-excited 1–3 transitions in Be-like O, for example transitions between levels associated with the $1s2p^23p$ and $1s^22p^2$ configurations. Similar transitions, as well as excited-excited inner-shell transitions in B-like O, also contribute weaker lines in the 20.5 to 20.8 Å range. Quite exotic transitions, such as between levels associated with the $1s^24d$ and $1s2p5d$ configurations in Li-like O, are found to contribute spectral lines around 21.0 Å. Such transitions involving two-electron jumps can only arise through significant configuration-interaction effects in the structure calculation. It was also realized that, although calculations for this colder and denser plasma produced the desired spectral features in the 20.0 to 21.0 Å wavelength range, such a plasma could not fully describe all the spectral features found in the experiment. The calculation at 60 eV and with an electron density of 5×10^{22} cm^{-3} produces a plasma in which the Li-like stage is dominant, and so the intensity of the He-like and H-like lines does not match the experimental spectrum well.

These investigations support the following scenario: most of the O line emission comes from a plasma that is quite hot and moderately dense (in the 100–150

eV electron temperature and $\sim 3.6 \times 10^{20}$ cm^{-3} electron density ranges), but a small portion of the experimental spectrum arises from a colder and denser region of the plasma that may surround the focal spot. The hotter, less dense region contributes most of the intense spectral features found in the experiment, but the colder, denser region also contributes to the observed spectra in the 20.0 to 21.0 Å range, and the lines are noticeable due to the high electron density of this region. We subsequently computed a "mixed" spectrum using ATOMIC, which arises from a plasma comprised of a 99% hot, less dense region (at $T_e = 150$ eV and $N_e = 3.6 \times 10^{20}$ cm^{-3}) and 1% of a colder, denser region (at $T_e = 60$ eV and $N_e = 5 \times 10^{22}$ cm^{-3}). This spectrum is shown in Fig. 3 and compared to the experimental spectrum from [1]. We have subtracted a constant background from the measurements to more easily compare the weaker lines in the 20–21.5 Å region. In this case, Voigt, rather than Gaussian, line profiles are used in the ATOMIC calculations, and we include full Stark broadening effects in the line shapes for the H-like and He-like lines, all to better compare with the experimental spectrum. We find the agreement to be quite reasonable, although some discrepancies persist. The ATOMIC calculation reproduces the main features of the measured spectrum, namely the Lyman and He-like series, as previously discussed. It also produces dielectronic satellite lines of similar intensity to the observed lines in the 19.1 to 19.6 Å wavelength range. This calculation also produces a spectrum of comparable intensity to the experimental result in the 19.8 to 21.0 Å range. However, the ATOMIC line positions in this wavelength range are slightly different from the experimental lines, with a difference of around 0.2 Å. Since the ATOMIC line positions of most of the other He-like and H-like lines are in very good agreement with experiment, this difference is unlikely to be due to a wavelength calibration issue. Rather, it is possible that the structure calculations

for the excited levels within the Be-like and B-like O ion stages may be less accurate than the He-like and H-like results. Our structure calculations (as discussed in the previous section) are performed with the CATS code, which is based on Cowan's Hartree-Fock approach [14]. An inaccuracy of only 1% would be enough to change the wavelength positions by around 0.2 Å, and such an inaccuracy is plausible for such excited levels of moderately ionized O. Increasing the accuracy of these calculations may require significantly more configuration-interaction effects, which implies a much larger overall calculation. Unfortunately, atomic databases that contain accurate energy levels for (doubly) excited levels of moderately ionized ions are very sparse, and so it is difficult to independently assess the accuracy of our atomic structure calculations for these ion stages.

We also note that the intensity of the Lyman-α and He-α lines predicted by ATOMIC is greater than that found experimentally. These lines are expected to be quite sensitive to opacity broadening effects (which have not been included in the ATOMIC calculations), which would broaden the lines and lower their peak intensity. We do note that the calculations and measurements are in good agreement for the other lines in the He-like series, which are less sensitive to opacity broadening effects. Finally, we also find that the ATOMIC "mixed" calculations predict strong lines in the 22.0–22.4 Å range. These lines arise from 1–2 transitions in Li-like O, and are enhanced due to the presence of the colder, denser plasma region. The measured spectrum also contains lines in this wavelength range, although they are much weaker.

To further support our hypothesis that the line emission in the observed plasma arises from two distinct regions, we also present in figure 4 2D radiation-hydrodynamic simulations using the HYDRA code [22]. The left-hand panels

of figure 4 show the temperature profile of the plasma at two times and the right-hand panels show the electron density profile at the same times. The laser and target parameters of the simulations were chosen to be representative of the experiment. In figure 4, the target is positioned at 0 μm, with the laser incident from the right-hand side. The peak of the laser pulse was at a time $t_0 = 0.287$ ns, and the simulations are shown for two times as indicated. The simulations show that, at 0.5 ns, the central portion of the target surface is hot (100s of eV) and moderately dense, since the laser has removed most of the target in the focal region. The outer regions of the target are substantially cooler, but remain at near solid density. At later times, the target cools quickly (to $\sim$40 eV in the focal region). The lower ionization stages of O are present near the cooler, more dense regions near the edge of the focal region. Further spatially resolved analysis (not shown) indicates that the satellite and continuum lines originate at the target surface while the resonance lines arise from the lower density portions.

The measurement of the intrinsic line shape for different plasma conditions is important for comparisons with opacity codes and to determine the effect on the Rosseland mean opacity. The main objective of the experimental study was to measure the far wing line shape in a low optical depth part of the spectrum. This is a challenging measurement since there is a requirement for high instrumental dynamic range and high spectral resolution to be able to determine the low intensity wing with 0.1–1% intensity of the line peak merging with the continuum. The high spectral resolution requirement gives the ability to resolve and distinguish weak line features. In addition, there are gradients along the line of sight as well as the usual issues of determining the plasma conditions accurately. This experimental and theoretical study

shows that there is more than the line wing to consider. The presence of line features from doubly excited transitions of lower ionization stages of oxygen indicates that this is a more complicated problem. Small fractions of lower-ionization stages in the cooler, denser plasma at the target surface and possibly surrounding the focal spot can add additional line structure to the wing.

Finally, we also considered whether the possible presence of hot electrons in the plasma could affect the observed spectra. At the experimental intensities used here, a hot electron component with temperature approaching 10 keV is possible, although the fraction of laser energy coupled into a hot electron component will be low. If such hot electrons influenced the observed spectra one would expect to see 2–1 transitions from low ionization states of O at the long wavelength side of the He-like 2–1 transition. However, such a line is not observed, and so we conclude that hot electrons do not influence the observed spectra presented here.

5 Conclusions

In this paper we have used the Los Alamos plasma kinetics code ATOMIC to produce emission spectra of O at several densities and temperatures. We use this capability to compare with recently observed laser-produced spectra [1] and postulate that the unexpected spectral features found in the measured spectrum from a Mylar target are due to exotic excited-excited inner-shell transitions in mid-ionized O. The high dynamic range of the spectrometer allows the detection of the weak exotic satellite lines. We note that further analysis of the Mylar foils used in the experiment, using a bulk element analysis technique, found no contaminants above the 50 ppm level by weight and most

were below 10 ppm. At this concentration level emission features would be well below the detection threshold of the instrument. Secondly those contaminants did not have identifiable emission features in this region. Therefore, we assert that the observed spectrum arises from plasma with two distinct regions: a hot, moderately dense bulk plasma responsible for the majority of the spectral features, and a region of cold, dense plasma that contributes weak spectral lines in the 20.0 to 21.0 Å range. We emphasize that our aim in this paper is to show that the cold, dense region can contribute spectral lines in the wavelength range examined here, and so we do not undertake a detailed study of the experimental gradients. Our assertion is consistent with the finding that the unexpected transitions were observed from a Mylar target and not an aerogel target. The Mylar target starts at solid density, unlike the aerogel structure, and so the plasma density will initially be much denser for the Mylar target. Finally, our hypothesis is further supported by 2D radiation-hydrodynamics simulations, which indicate a hot, less dense target region in the focal spot, and a cooler, more dense region at the edges of the focal spots.

Progress has been made in studying these features and by identifying the likely ionization stages and conditions. The next steps would be to perform a detailed comparison with the experimental data, by identifying specific transitions and further improving the atomic models by adding significantly more configuration-interaction effects, for the doubly excited levels. On the experimental front, detailed characterization of the plasma conditions using spatially resolved measurements and the use of spatially localized target materials, e.g. microdots, may be useful in determining the origin of this emission region. Varying the initial density of the target material may also prove to be useful and indicate a density sensitivity.

6 Acknowledgments

The authors would like to thank S. Hansen for initial atomic kinetic calculations. Thanks go to E. Magee, K. Cone, L. Elberson, J. Emig, J. Hunter, for experimental, technical and laser support as well as C. Cadwalader and R. Van Maren for target fabrication. The help of the Jupiter Laser Facility staff is appreciated. The Los Alamos National Laboratory is operated by Los Alamos National Security, LLC for the National Nuclear Security Administration of the U.S. Department of Energy under Contract No. DE-AC52-06NA25396. A portion of this work performed under the auspices of the U.S. Department of Energy by Lawrence Livermore National Laboratory under Contract DE-AC52-07NA27344.

References

[1] J. Dunn, E.W. Magee, R. Shepherd, H. Chen, S.B. Hansen, S.J. Moon, G.V. Brown, M.F. Gu, P. Beiersdorfer, M.A. Purvis, Rev. Sci. Instrum. 79 (2008) 10E314.

[2] C. Bowen, R. W. Lee, Yu. Ralchenko, J. Quant. Spectrosc. Radiat. Transfer 99 (2006) 102.

[3] J.G. Rubiano, R. Florido, C. Bowen, R.W. Lee, Yu. Ralchenko, High Energy Dens. Phys. 3 (2007) 225.

[4] C.J. Fontes, J. Abdallah, Jr., C. Bowen, R.W. Lee, Yu. Ralchenko, High Energy Dens. Phys. 5 (2009) 15.

[5] J.E. Bailey, G.A. Rochau, C.A. Iglesias, J. Abdallah, Jr., J.J. MacFarlane, I. Golovkin, P. Wang, R.C. Mancini, P.W. Lake, T.C. Moore, M. Bump, O. Garcia,

S. Mazevet, Phys. Rev. Letts. 99 (2007) 265002.

[6] C.A. Iglesias and B. Wilson, private communication (2008).

[7] N.J. Peacock, M.G. Hobby, M. Galanti, J. Phys. B 6 (1973) L298-304.

[8] L.A. Vainshtein and U.I Safronova, At. Data and Nucl. Data Tables 21 (1978) 49.

[9] J. Dunn, Y. Li, A.L. Osterheld, J. Nilsen, J.R. Hunter, V.N. Shlyaptsev, Phys. Rev. Letts. 84 (2000) 4834.

[10] N.H. Magee, J. Abdallah, Jr., J. Colgan, P. Hakel, D.P. Kilcrease, S. Mazevet, M. Sherrill, C.J. Fontes, H.L. Zhang, in *14th Topical Conference on Atomic Processes in Plasmas* (Eds: J.S. Cohen, S. Mazevet, and D.P. Kilcrease, AIP Conference Proceedings, New York, 2004) pp. 168–179.

[11] R.L. Kelly, J. Phys. Chem. Ref. Data 16 (1987) 1-1678.

[12] S.B. Hansen, private communication (2008).

[13] J. Abdallah, Jr., R.E.H. Clark, R.D. Cowan, Los Alamos National Laboratory, Los Alamos Manual No. LA 11436-M-I (1988).

[14] R.D. Cowan, *The Theory of Atomic Structure and Spectra* (University of California Press, Berkeley, 1981).

[15] R.E.H. Clark, J. Abdallah, Jr., J.B. Mann, Ap. J. 381 (1991) 597.

[16] R.E.H. Clark, J. Abdallah, G. Csanak, J.B. Mann, R.D. Cowan, Los Alamos National Laboratory, Los Alamos Manual No. LA 11436-M-II (1988).

[17] G. Csanak, H.S. Taylor, R. Yaris, Phys. Rev. A 3 (1971) 1322.

[18] G. Csanak, H.S. Taylor, R. Yaris, Adv. At. Mol. Phys. 7 (1971) 287.

[19] J. Colgan, J. Abdallah, Jr., A. Faenov, T.A. Pikuz, I.Yu. Skobelev, Physica Scripta 78 (2008) 015302.

[20] J. Colgan, J. Abdallah, Jr., A.Ya. Faenov, A.I. Magunov, T.A. Pikuz, I.Yu. Skobelev, Y. Fukuda, Y. Akahane, M. Aoyama, N. Inoue, H. Ueda, K. Yamakawa, Laser and Particle Beams 26 (2008) 83.

[21] T.C. Berkelbach, J. Colgan, J. Abdallah, Jr., A.Ya. Faenov, T.A. Pikuz, Y. Fukuda, K. Yamakawa, Phys. Rev. E 79 (2009) 016407.

[22] M.M. Marinak, S.W. Haan, T.R. Dittrich, R.E. Tipton, G.B. Zimmerman, Physics of Plasmas 5 (1998) 1125.

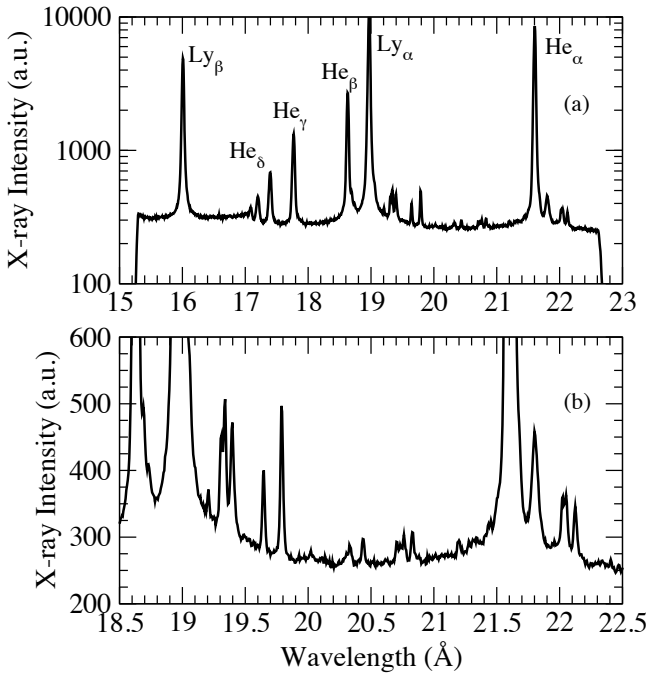

Fig. 1. Experimental spectra from [1] for a 3 μm thick Mylar foil. The upper panel shows a logarithmic plot of the spectra and the lower panel is provided to emphasize the features between 20 and 21.5 Å.

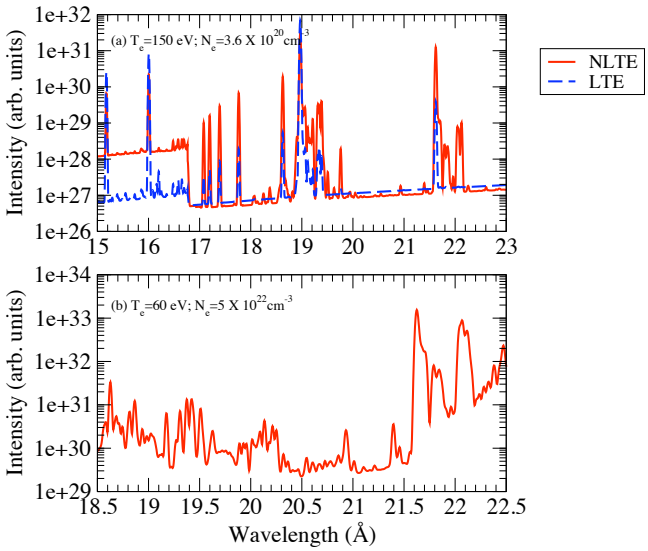

Fig. 2. Theoretical spectra computed using ATOMIC. The upper panel shows LTE and NLTE ($T_r = 0$) spectra for the conditions $T_e = 150$ eV and $N_e = 3.6 \times 10^{20}$ cm^{-3} as indicated. The lower panel shows a NLTE ($T_r = 0$) spectrum for the conditions $T_e = 60$ eV and $N_e = 5 \times 10^{22}$ cm^{-3}.

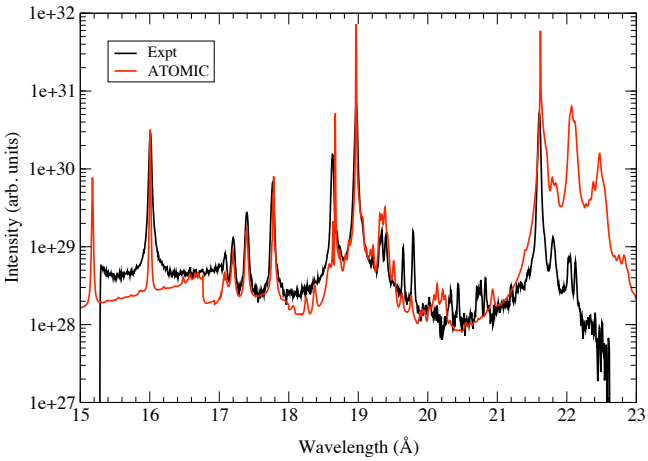

Fig. 3. ATOMIC 'mixed' spectra, comprised of 99% of the hot, less dense region (with $T_e = 150$ eV and $N_e = 3.6 \times 10^{20}$ cm^{-3}), and 1% of the colder, denser region ($T_e = 60$ eV and $N_e = 5 \times 10^{22}$ cm^{-3}). Stark broadening of the H-like and He-like lines has been included in the ATOMIC calculations, and a Voigt profile used for the other line shapes.

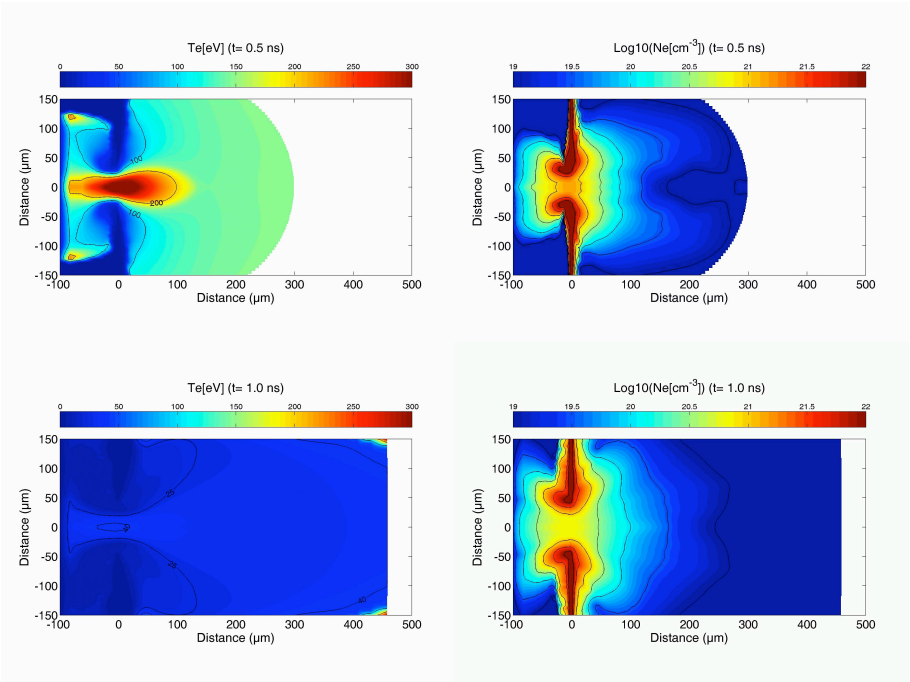

Fig. 4. 2D Hydrodynamic simulations using the HYDRA code [22] at two times. The left-hand panels show the temperature profile of the plasma at 0.5 and 1.0 ns, and the right-hand panels show the electron density profile at the same times.